

**$\beta$ -arrestin-1 contributes to brown fat function  
and directly interacts with PPAR $\alpha$  and PPAR $\gamma$**

Congcong Wang<sup>1,2</sup>, Xianglu Zeng<sup>1,5</sup>, Zhaocai Zhou<sup>1</sup>, Jian Zhao<sup>1,4,\*</sup>, Gang Pei<sup>1,3,\*</sup>

<sup>1</sup> *State Key Laboratory of Cell Biology, Institute of Biochemistry and Cell Biology, Shanghai Institutes for Biological Sciences, Chinese Academy of Sciences, 320 Yueyang Road, Shanghai 200031, China*

<sup>2</sup> *Graduate School, University of Chinese Academy of Sciences, Chinese Academy of Sciences, 320 Yueyang Road, Shanghai 200031, China*

<sup>3</sup> *School of Life Science and Technology, Tongji University, Shanghai 200092, China*

<sup>4</sup> *Translational Medical Center for Stem Cell Therapy, Shanghai East Hospital, School of Medicine, Tongji University, Shanghai 200120, China*

<sup>5</sup> *Shanghai Key Laboratory of Signaling and Disease Research, Laboratory of Receptor-based Bio-medicine, School of Life Sciences and Technology, Tongji University, Shanghai 200092, China*

*\* Correspondence and requests for materials should be addressed to Gang Pei (email: gpei@sibs.ac.cn) and Jian Zhao (email: jzhao@sibcb.ac.cn).*

## Supplementary Information

### Supplementary Figures

Figure S1 Targeted disruption of *Arrb1* gene in Mice.

Figure S2 Body weights and blood glucose levels of the *Arrb1*-KO mice and their wild-type littermates.

Figure S3 Kinetic analysis for different immobilization levels of PPAR $\alpha$ , PPAR $\gamma$  and RXR $\alpha$ .

Figure S4 Comparison of the fitting models on the binding curves of PPAR $\alpha/\gamma$ -LBD with  $\beta$ -arrestin-1 or RXR $\alpha$ -LBD.

Figure S5 The kinetics of  $\beta$ -arrestin-1 binding to PPAR $\alpha$ -LBD and PPAR $\gamma$ -LBD in the presence of RXR $\alpha$ -LBD.

Figure S6 The kinetics of G $\alpha$ s binding to  $\beta$ -arrestin-1 and  $\beta$ arr1M.

Figure S7 Effects of  $\beta$ -arrestin-1 peptide on the interactions between RXR $\alpha$ -LBD and PPAR $\alpha/\gamma$ -LBD.

Figure S8 The kinetics of PPAR $\alpha/\gamma$ -LBD binding to  $\beta$ -arrestin-1 peptide mutants.

Figure S9 The kinetics of  $\beta$ arr1M binding to PPAR $\gamma$  M1 and M2.

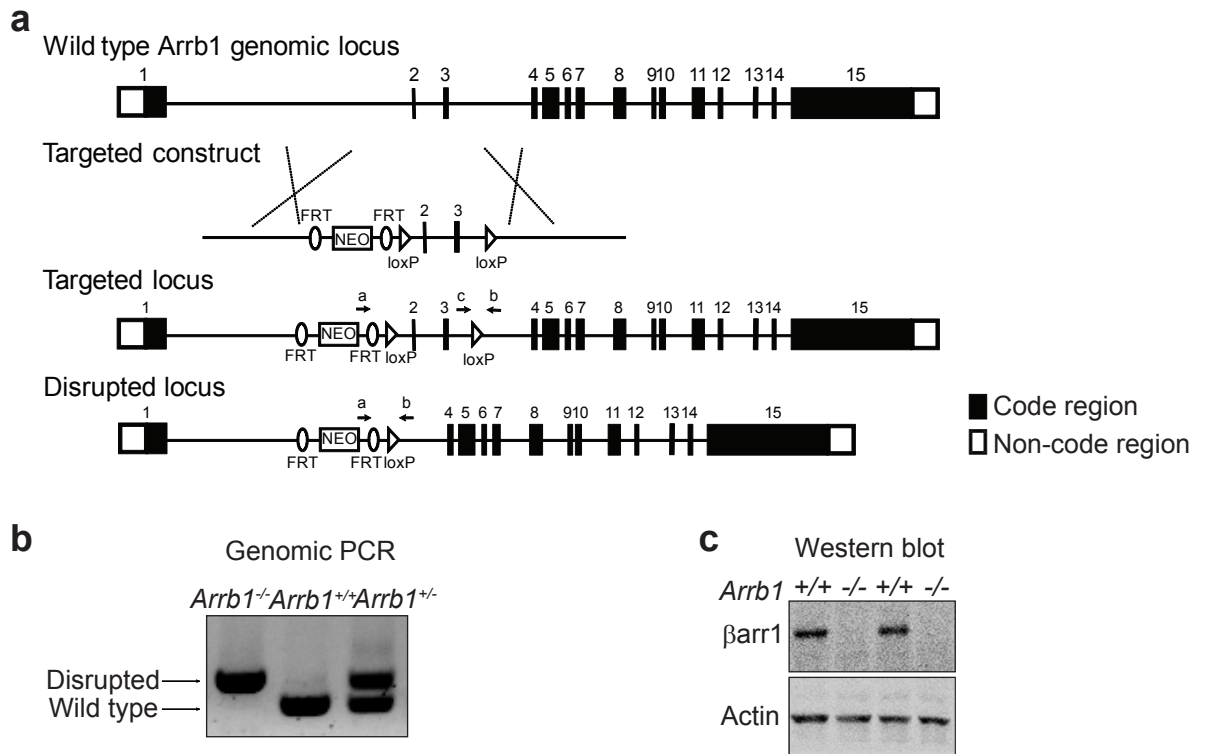
Figure S10 The residual plots for the fitting curves in Fig. 3 and Fig. 4.

Figure S11 Full-length blots for Fig. 2 and Fig. 3.

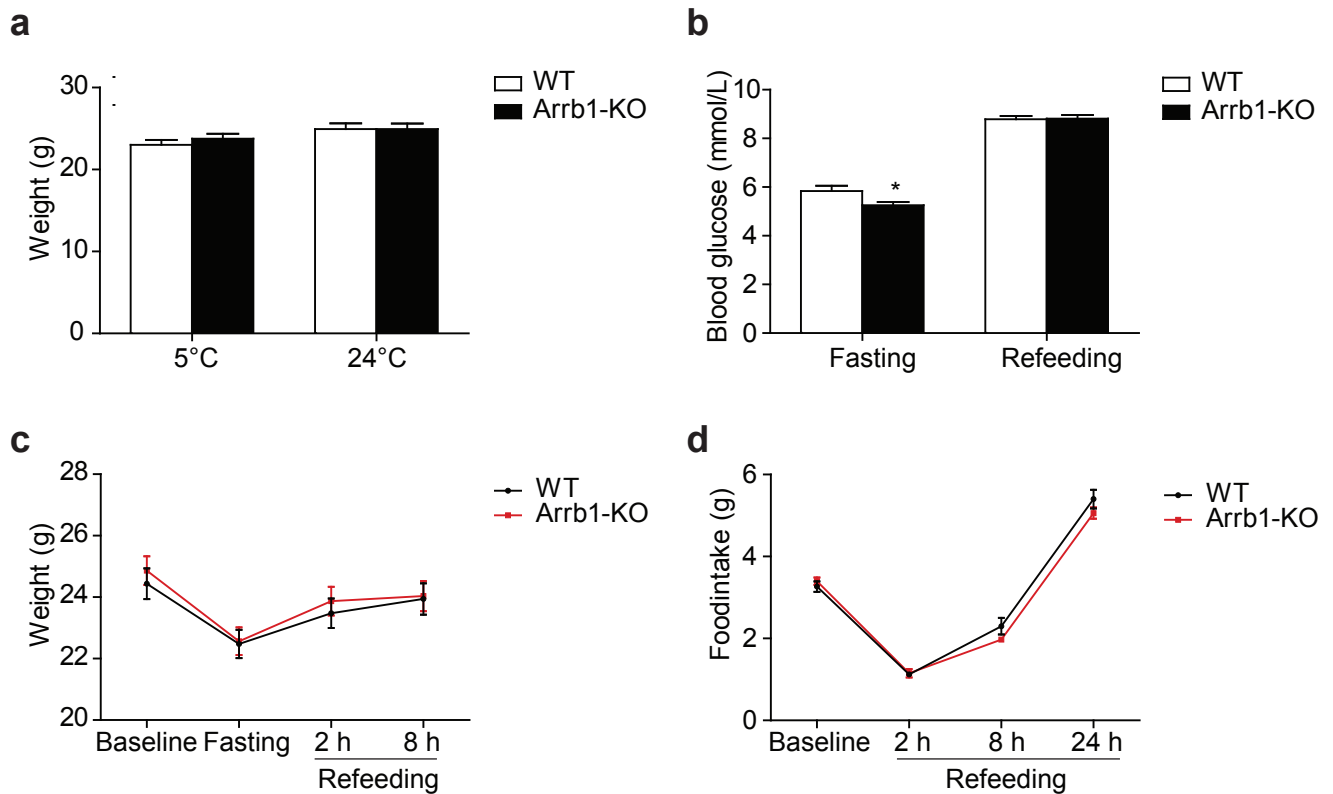
### **Supplementary Table**

Table S1 Primer List for RT-PCR.

Table S2 Molecular Weight (MW) of the indicated proteins and peptides.



**Figure S1. Targeted disruption of *Arrb1* gene in Mice.** (a) Schematic of *Arrb1* gene-targeting strategy. Excision of the sequences between the loxP sites by the *Cre* recombinase deletes 2-3 exons in *Arrb1*. The locations of the primers a, b, and c used for genomic PCR analysis are indicated. (b) Representative PCR analysis of genomic DNA from the homozygous, wild-type and heterozygous mice. The migrated position of the fragments derived from the wild-type and disrupted alleles are indicated. (c) Western blot analysis of the expression of β-arrestin-1 in BAT of the wild-type and *Arrb1*-KO mice.



**Figure S2. Body weights and blood glucose levels of the Arrb1-KO mice and their wild-type littermates.** (a) Body weights of the wild-type (n=13) and Arrb1-KO (n=13) mice for each group exposed to either 5°C or 24°C. Data are shown as means  $\pm$  S.E.M. (b) Blood glucose levels of the wild-type (n=25) and Arrb1-KO (n=25) mice after fasting and refeeding. Mice were fasted for 16 h (from 17:00 to 9:00) and then refed with a regular chow diet for 2 h (9:00-11:00). Data are presented as means  $\pm$  S.E.M. \*,  $p < 0.05$  versus the wild-type group. (c) Body weights of the wild-type (n=20) and Arrb1-KO (n=20) mice after fasting for 16 h and refeeding for 2 h or 8 h. Mice were fasted for 16 h (from 17:00 to 9:00) and then refed with a regular chow diet for 8 h (9:00-17:00). Data are presented as means  $\pm$  S.E.M. (d) Food intakes of the wild-type (n=14) and Arrb1-KO (n=14) mice after refeeding for 2 h, 8 h, and 24 h. Mice were fasted for 16 h (from 17:00 to 9:00) and then refed with a regular chow diet for 24 h. Data are presented as means  $\pm$  S.E.M.

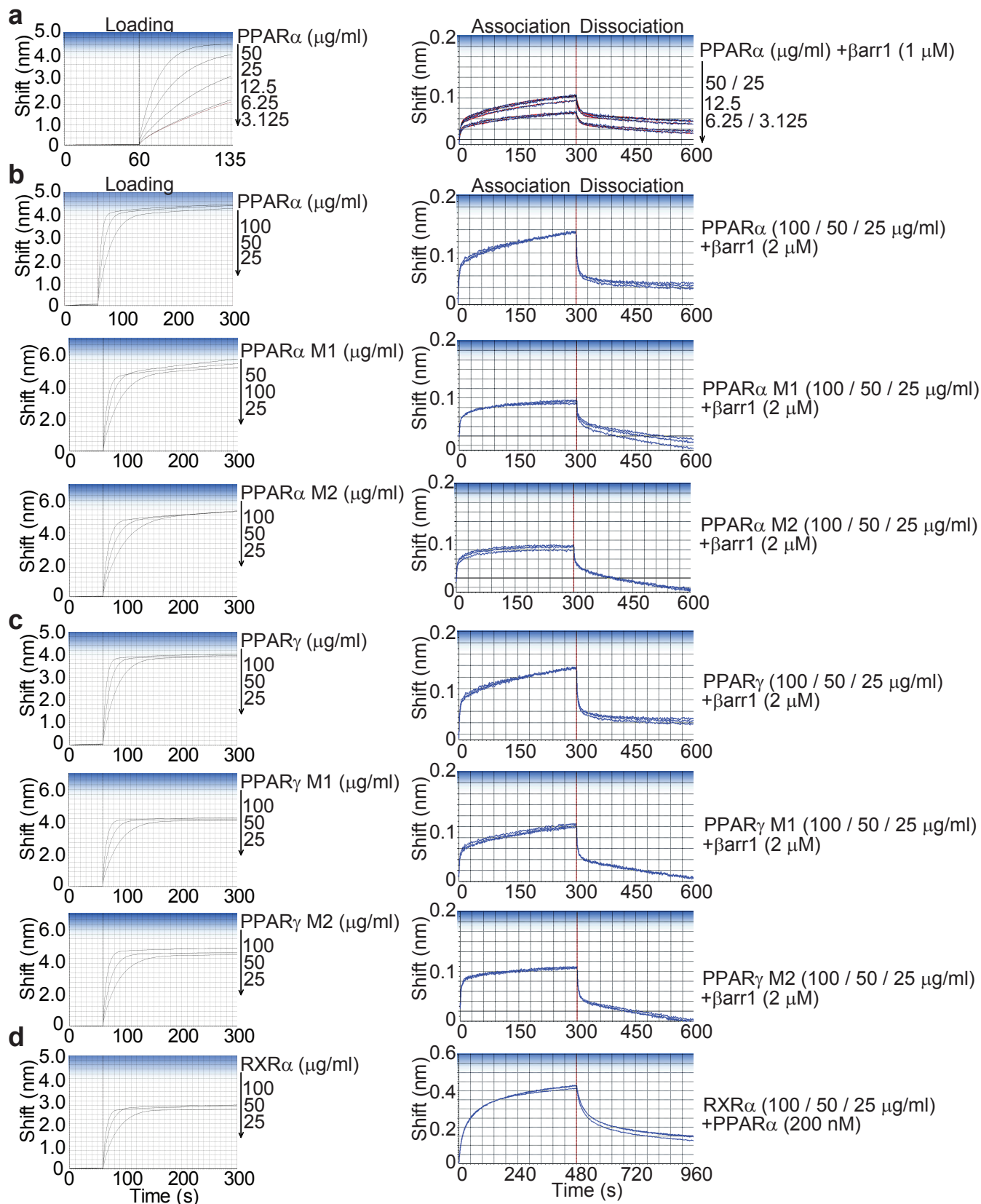


**Figure S3. Kinetic analysis for different immobilization levels of PPAR $\alpha$ , PPAR $\gamma$  and RXR $\alpha$ .** (a) Biolayer interferometry analysis for the interaction of PPAR $\alpha$  with  $\beta$ -arrestin-1. Streptavidin biosensors (SAs) were immobilized with 50-3.125  $\mu\text{g/ml}$  biotinylated PPAR $\alpha$ -LBD for 70 s. The SAs were then incubated with 1  $\mu\text{M}$   $\beta$ -arrestin-1 at 25 $^{\circ}\text{C}$ . (b, c) Kinetic analysis for the interaction of PPAR $\alpha/\gamma$  with  $\beta$ -arrestin-1. Purified 100-25  $\mu\text{g/ml}$  biotinylated wild-type PPAR $\alpha/\gamma$ -LBD, PPAR $\alpha/\gamma$  M1 and M2 were loaded onto the SAs for 240 s, and then incubated with 2  $\mu\text{M}$   $\beta$ -arrestin-1 at 25 $^{\circ}\text{C}$ . (d) Kinetic analysis for the interaction of RXR $\alpha$ -LBD with PPAR $\alpha$ -LBD. Purified 100-25  $\mu\text{g/ml}$  biotinylated RXR $\alpha$ -LBD were immobilized onto the SAs for 240 s and incubated with 200 nM PPAR $\alpha$  at 25 $^{\circ}\text{C}$ . All the association/dissociation curves were shown on the right.

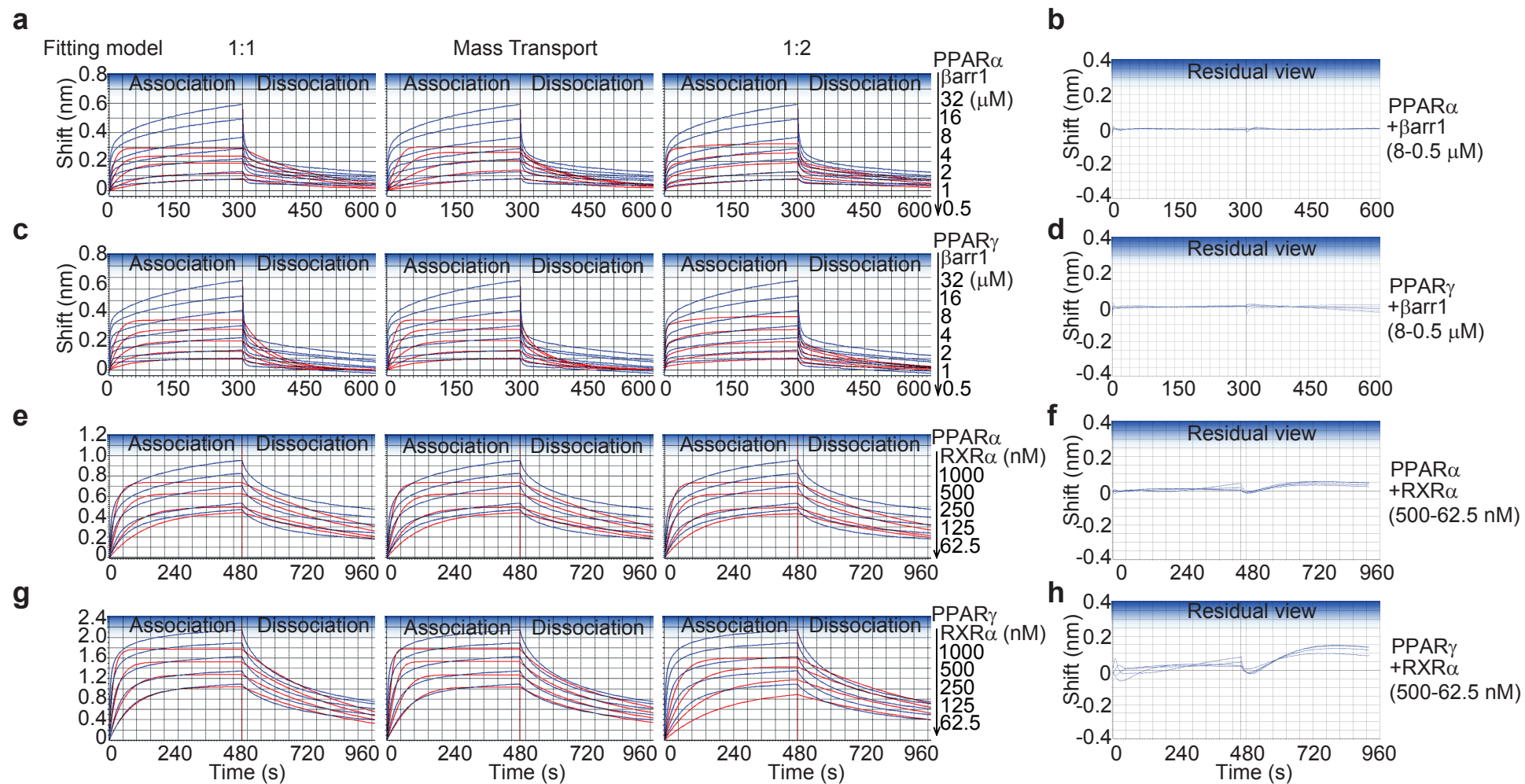


**Figure S4. Comparison of the fitting models on the binding curves of PPAR $\alpha/\gamma$ -LBD with  $\beta$ -arrestin-1 or RXR $\alpha$ -LBD. (a-d)** The binding curves of PPAR $\alpha$ -LBD or PPAR $\gamma$ -LBD with  $\beta$ -arrestin-1 were fitted using the 1:1, Mass Transport, and 1:2 BA models. The residual plots generated from a 2:1 HL model were shown on the right. **(e-h)** The binding curves of PPAR $\alpha$ -LBD or PPAR $\gamma$ -LBD with RXR $\alpha$ -LBD were fitted using the 1:1, Mass Transport, and 1:2 BA models. The residual plots generated from a 2:1 HL model were shown on the right. The experimental data are represented by blue lines and the curve fitting data are indicated by red lines.

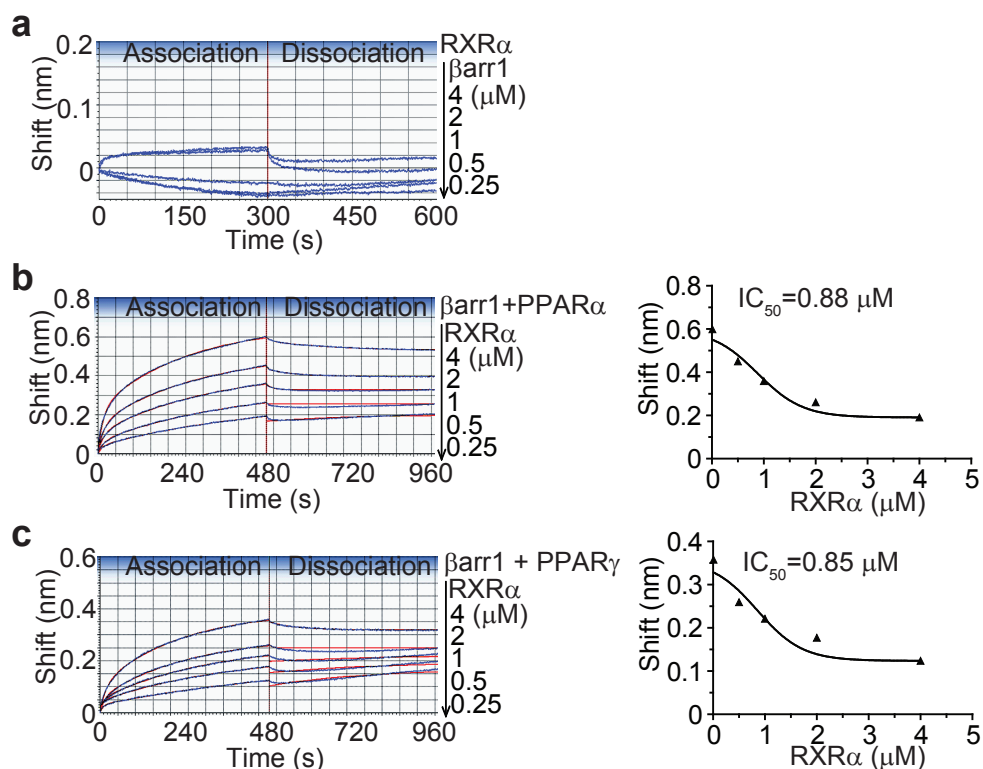


**Figure S5. The kinetics of  $\beta$ -arrestin-1 binding to PPAR $\alpha$ -LBD and PPAR $\gamma$ -LBD in the presence of RXR $\alpha$ -LBD.** (a) Biolayer interferometry analysis of the interaction between  $\beta$ -arrestin-1 and RXR $\alpha$ -LBD. Streptavidin biosensor (SA) immobilized with 50  $\mu$ g/ml biotinylated RXR $\alpha$ -LBD was incubated in wells containing different concentrations of purified  $\beta$ -arrestin-1 at 25°C. (b, c) The kinetics of  $\beta$ -arrestin-1 binding to PPAR $\alpha$ -LBD and PPAR $\gamma$ -LBD in the presence of RXR $\alpha$ -LBD. Purified 50  $\mu$ g/ml  $\beta$ -arrestin-1 was loaded on SAs and incubated with 200 nM PPAR $\alpha$ -LBD and PPAR $\gamma$ -LBD in the presence of a serial dilution of RXR $\alpha$ -LBD at 25°C. The IC<sub>50</sub> values were estimated from the plots of maximum responses versus concentrations.



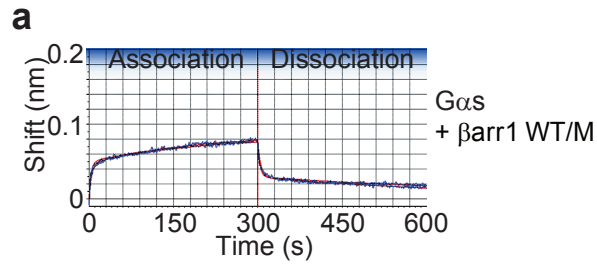


**Figure S6. The kinetics of  $G\alpha_s$  binding to  $\beta$ -arrestin-1 and  $\beta arr1M$ .** (a) Biolayer interferometry analysis of the interactions between  $G\alpha_s$  and  $\beta$ -arrestin-1 or  $\beta arr1M$ . Streptavidin biosensors immobilized with 50  $\mu g/ml$  biotinylated  $G\alpha_s$  were incubated with 2  $\mu M$   $\beta$ -arrestin-1 or  $\beta arr1M$  at 25°C.

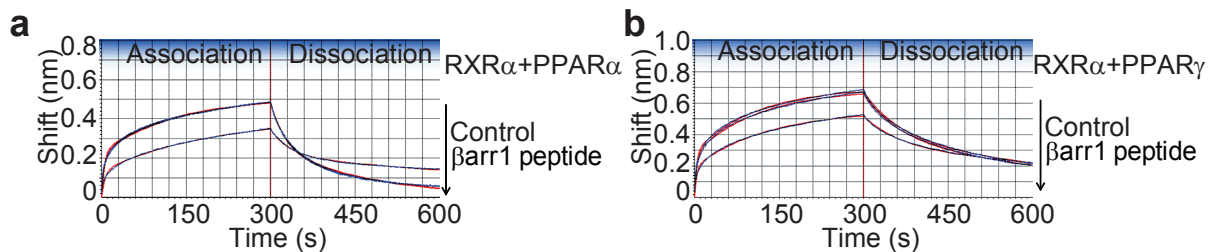


**Figure S7. Effects of  $\beta$ -arrestin-1 peptide on the interactions between RXR $\alpha$ -LBD and PPAR $\alpha/\gamma$ -LBD. (a, b)** The kinetics of RXR $\alpha$ -LBD binding to PPAR $\alpha$ -LBD and PPAR $\gamma$ -LBD in the presence of  $\beta$ -arrestin-1 peptide. 50  $\mu$ g/ml biotinylated RXR $\alpha$ -LBD was loaded on SAs and incubated with 200 nM PPAR $\alpha$ -LBD or PPAR $\gamma$ -LBD in the presence of 0.4 mM  $\beta$ -arrestin-1 peptide or an irrelevant peptide at 25°C.

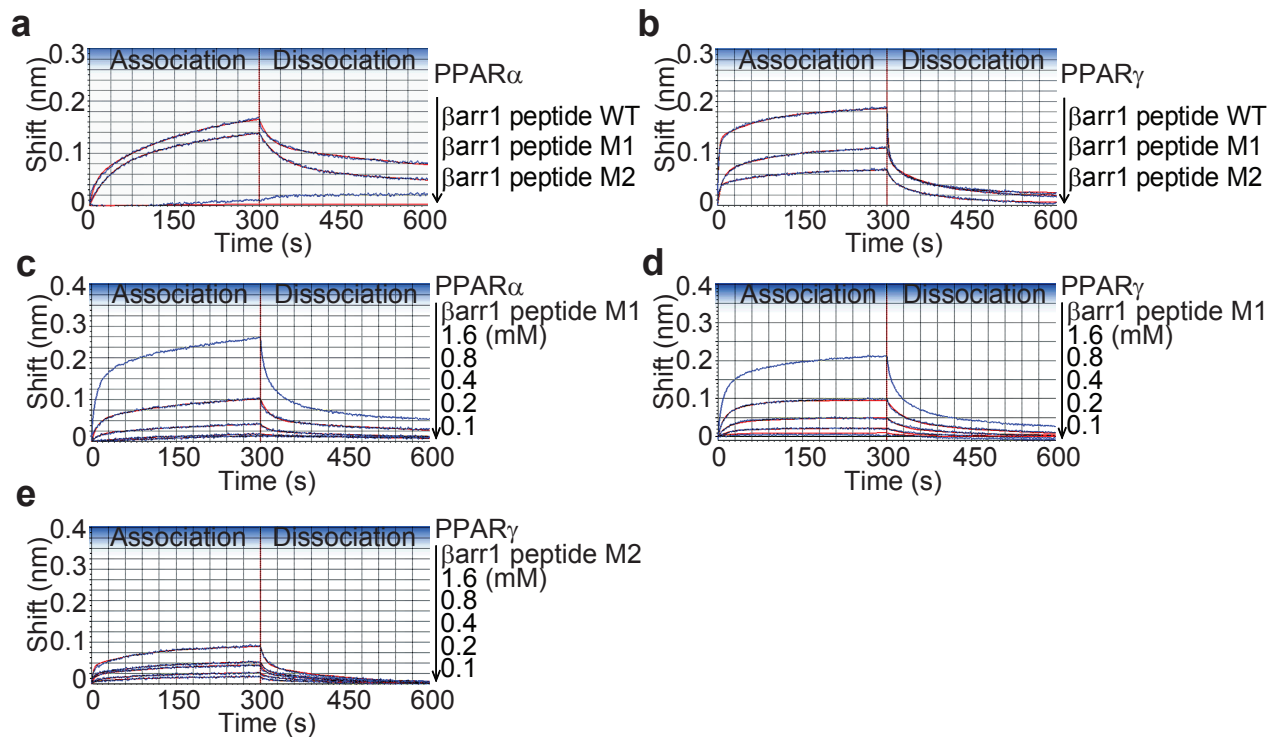


**Figure S8. The kinetics of PPAR $\alpha/\gamma$ -LBD binding to  $\beta$ -arrestin-1 peptide mutants.** (a, b) Biolayer interferometry analysis of the interactions between PPAR $\alpha/\gamma$ -LBD and  $\beta$ -arrestin-1 peptide M1 or M2. 50  $\mu$ g/ml PPAR $\alpha/\gamma$ -LBD-loaded SAs were incubated with 0.8 mM  $\beta$ -arrestin-1 peptide M1 or M2 at 25°C. (c, d, e) The kinetic analysis of PPAR $\alpha/\gamma$ -LBD binding to  $\beta$ -arrestin-1 peptide M1 or M2. Purified 50  $\mu$ g/ml PPAR $\alpha/\gamma$ -LBD were loaded on SAs and incubated with different concentrations of  $\beta$ -arrestin-1 peptide M1 or M2 at 25°C. The experimental data are represented by blue lines and the curve fitting data are indicated by red lines.

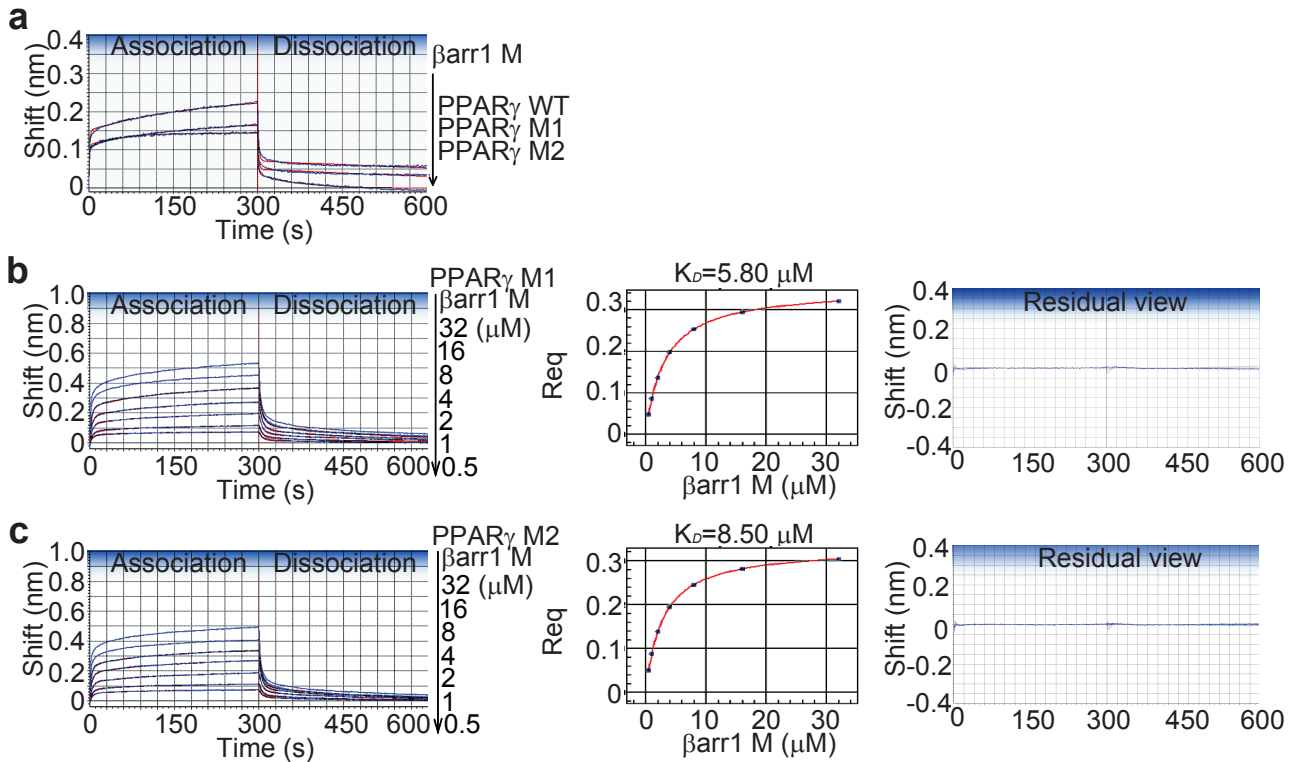


**Figure S9. The kinetics of  $\beta$ arr1M binding to PPAR $\gamma$  M1 and PPAR $\gamma$  M2.**

(a) Interactions between  $\beta$ arr1M and PPAR $\gamma$ -LBD L311G/N312G (PPAR $\gamma$  M1) or D380A (PPAR $\gamma$  M2) using the ForteBio Octet Red instrument. Purified 50  $\mu$ g/ml wild-type PPAR $\gamma$ -LBD, PPAR $\gamma$  M1, and PPAR $\gamma$  M2 were immobilized on SAs and incubated with 2  $\mu$ M  $\beta$ arr1M at 25°C. (b, c) The kinetic analysis of  $\beta$ arr1M binding to PPAR $\gamma$  M1 and PPAR $\gamma$  M2, respectively. The SAs immobilized with 50  $\mu$ g/ml PPAR $\gamma$  M1 and PPAR $\gamma$  M2 were incubated with different concentrations of purified  $\beta$ arr1M at 25°C. The steady state analysis and  $K_D$  of the binding curves were shown in the middle. The 2:1 HL model was used to fit the binding curves and the residual plots were shown on the right. The experimental data are represented by blue lines and the curve fitting data are indicated by red lines.

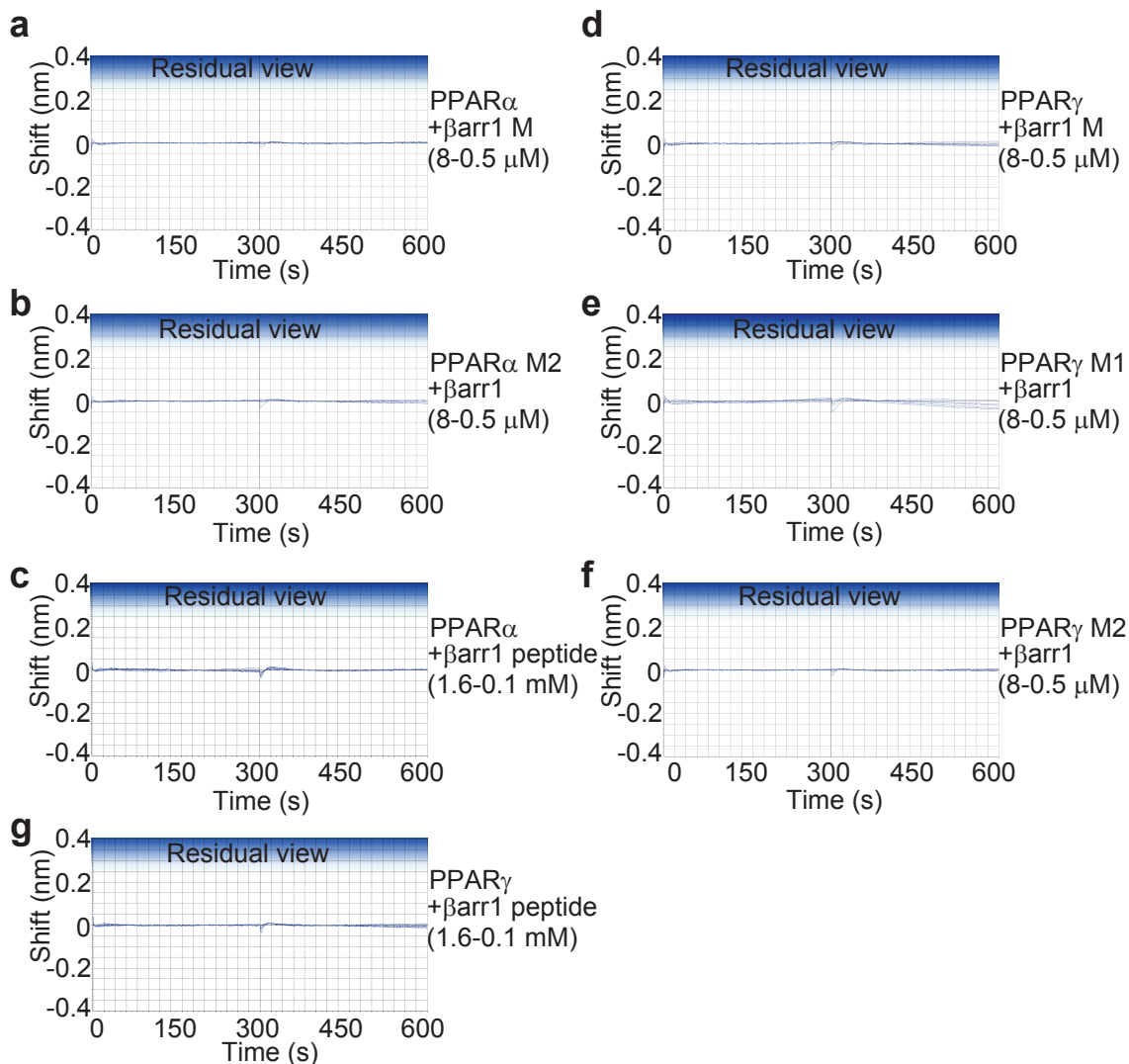


**Figure S10. The residual plots from the fitting curves in Fig. 3 and Fig. 4. (a, b, c)** The residual plots from the fitting curves of wild-type PPAR $\alpha$ -LBD or PPAR $\alpha$  M2 binding to  $\beta$ arr1 and  $\beta$ arr1 peptide. **(d-g)** The residual plots from the fitting curves of wild-type PPAR $\gamma$ -LBD, PPAR $\gamma$  M1 or PPAR $\gamma$  M2 binding to  $\beta$ arr1 and  $\beta$ arr1 peptide. The 2:1 HL model was used to fit all the binding curves.

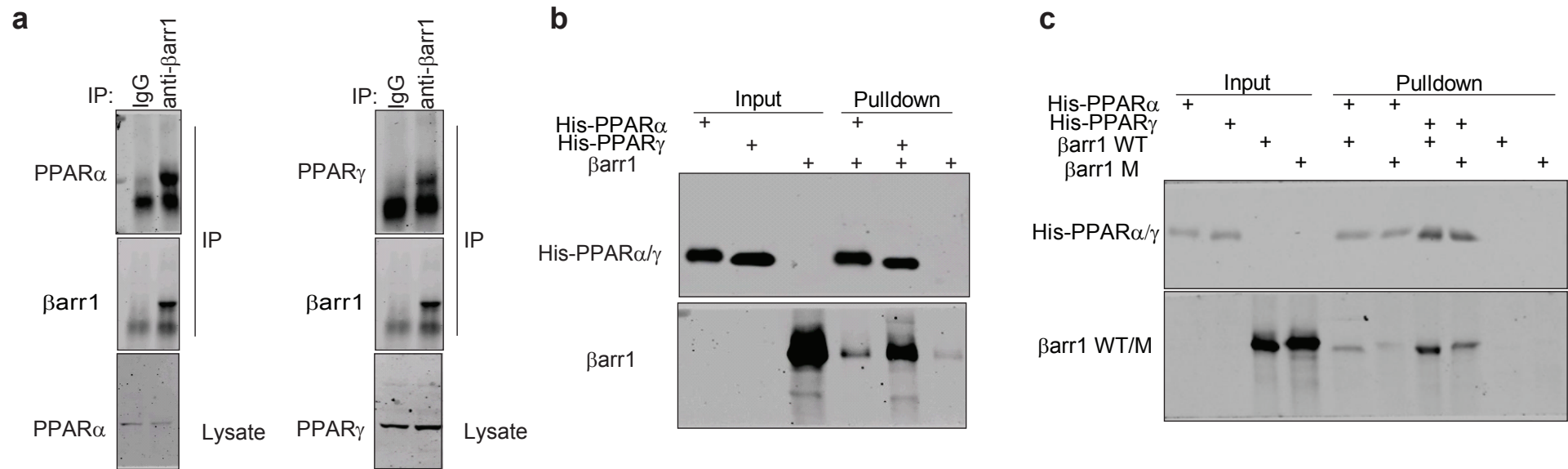


**Figure S11. Full-length blots for Fig. 2 and Fig. 3. (a)** Full-length blots for Fig. 2a. **(b)** Full-length blots for Fig. 2b. **(c)** Full-length blots for Fig. 3b.

## Supplementary Table

Table S1. Primer List for RT-PCR

<b>RT-PCR</b>	<b>Forward 5'→3'</b>	<b>Reverse 5'→3'</b>
Ucp1	CACCTTCCCCTGGACT	CCCTAGGACACCTTTATACCTAATGG
PGC1 $\alpha$	GCGCCGTGTGATTTACGTT	AAAACCTCAAAGCGGTCTCTCAA
PGC1 $\beta$	TCCTGTAAAAGCCCGGAGTAT	GCTCTGGTAGGGCAGTGA
Cox7a	CAGCGTCATGGTCAGTCTGT	AGAAAACCGTGTGGCAGAGA
CPT1 $\beta$	CTGTTAGGCCCTCAACACCGAAC	CTGTCATGGCTAGGCTGTACAT
Cidea	ATCACAACTGGCCTGGTTACG	TACTACCCGGTGTCCATTCT
PPAR $\alpha$	TCAGGGTACCACTACGGAGT	CTTGGCATTCTTCCAAAGCG
PPAR $\gamma$	GCATGGTGCCTTCGCTGA	TGGCATCTCTGTGTCAACCATG
Prdm16	CAGCACGGTGAAGCCATTC	GCGTGCATCCGCTTGTG

Table S2. Molecular Weight (MW) of the indicated proteins and peptide

<b>Proteins and peptides</b>	<b>MW (Dalton)</b>
PPAR $\alpha$ -LBD	30,865
PPAR $\alpha$ M1	30,751
PPAR $\alpha$ M2	30,821
PPAR $\gamma$ -LBD	31,283
PPAR $\gamma$ M1	31,170
PPAR $\gamma$ M2	31,239
$\beta$ -arrestin-1	47,019
$\beta$ arr1M	46,935
RXR $\alpha$ -LBD	26,823
$\beta$ -arrestin-1 peptide	2,431
$\beta$ -arrestin-1 peptide M1	2,263
$\beta$ -arrestin-1 peptide M2	2,495
The irrelevant peptide	2,688